Preliminary Results in using a Joint Contrast Enhancement and Turbulence Mitigation Method for Underwater Optical Imaging

Kristofor B. Gibson
SSC Pacific
53560 Hull St.
San Diego, CA 92152
Email: kris.gibson@navy.mil

***Abstract*—In this article, the author investigates the method of turbulence mitigation and contrast enhancement originally designed for atmospheric imaging for the purpose of improving underwater optical image sequences so operators can accomplish their task of object inspections more effectively by increasing the local contrast, reducing noise, mitigate marine snow, and increasing the sharpness. With video obtained in the San Diego bay, we present subjective and objective comparisons that show our proposed method is effective in improving perceptual quality and ultimately making the object inspection tasks easier for the operator.**

I. Introduction

The Sensor-Based Stabilized ROV for Water Borne IED (WBIED) Identification & Neutralization or SSR-WIN needs to inspect piers, pilings, and ship berthing areas as part of its worldwide mission with the US Navy. While the ROV conducts inspections, the operator is able to monitor the vehicles behavior, and the Automatic Target Recognition (ATR) system queues the operator to potential threats. At all times, the operator has the ability to pause a mission and further inspect an object of interest, then resume the mission back at the point where the mission was paused.

Unfortunately, the inspection of objects underwater with a video camera (color or monochrome) is a difficult task for operators. This difficulty is most prevalent in turbid water with low light conditions. Many factors degrade the perceptual quality of optical image sequences. Low light conditions, back scatter from diffuse light source, color dependent scattering and attenuation from turbid medium, blur, and marine snow (particulates in the water) are the main factors in degrading the perceptual quality of optical video.

Even in shallow water, low light conditions are possible due to structures surrounding the ROV which significantly lower the SNR of the object in a scene. In this particular case, SSR-WIN has two diffuse light sources to account for low-light scenarios. This active light source, however, introduces backscatter illumination since range-gating or polarizing is not implemented. The backscatter illumination is not wanted because although the object is illuminated, the scattering medium is also illuminated which ultimately lowers the contrast and SNR of the optically imaged object.

Light scattering and attenuation in a medium has been studied for years and accurately modeled [1]–[4]. This physical phenomenon must be addressed in underwater imaging because of the degradation in contrast of the optically imaged object. The light radiating from the object is scattered over distance exponentially as well as absorbed by the water and suspended materials over distance. Thus, depending on the type of scattering, there is a specific range limitation to optical imaging objects underwater. Marine snow degrades the view of the objects in optical imaging sequences by obstructing local regions. With the assumption that marine snow is flowing through the water at random distances and velocities, a common approach to mitigating marine snow is to temporally average an image sequence to generate a single image. This method of statistically averaging frames, however, introduces global blur. We show in this article that the blur degradation is statistically similar to atmospheric turbulence blur observed with long exposure imaging systems.

With the exception of attenuation, the degradations encountered when imaging underwater are very similar to imaging in the atmosphere such that there is SNR issues in low light, low contrast, and blur. Therefore enhancement methods designed for imaging in the atmosphere may also improve optical imaging results. In this article, the Contrast Enhancement Turbulence Mitigation (CETM) method [5] is applied to the SSR-WIN's optical imaging system. Due to differences in physics, the CETM is modified to accommodate those differences. These differences are discussed in the next section.

A. Imaging Model

Let's begin with the following imaging model,

$$i_k(\mathbf{x}) = h_k(\mathbf{x}) * \Big(t_k(\tilde{\mathbf{x}}_k)o_k(\tilde{\mathbf{x}}_k) + (1 - t_k(\tilde{\mathbf{x}}_k))w + l(\tilde{\mathbf{x}}_k)b_k(\tilde{\mathbf{x}}_k)\Big) + n_k(\mathbf{x}), \quad (1)$$

which is a very similar model used for atmospheric imaging. The subscript, k, denotes the time or frame number for a video sequence. The monochromatic image $i(\mathbf{x}) \in \mathbb{R}$, at the two dimensional spatial location is $\mathbf{x} \in \mathbb{R}^2$. The point spread function (PSF) which consists of the entire optical imaging path (medium and optics) is h. The relative motion of the sensor system and object is modeled with

$$\tilde{\mathbf{x}}_k = \Delta_{g,k} + \Delta_{l,k}(\mathbf{x}), \quad (2)$$

where $\Delta_{g,k}$ is the global motion and $\Delta_{l,k}(\mathbf{x})$ is local motion. The contrast degradation is due to the $t_k \in \mathbb{R}$ and $w \in \mathbb{R}$ terms which are discussed in detail in the following section. The object image without any degradations is $o_k(\mathbf{x}) \in \mathbb{R}$. Therefore the goal in this article is to recover $o_k(\mathbf{x})$ given multiple observations $i_k(\mathbf{x})$. The backscatter which is the illumination of the medium by a light source (or more) near the imaging optics and illuminated marine snow is encapsulated in the term $b(\mathbf{x})$. The weighting term, $l(\mathbf{x})$ is used to account for active lighting from the sensor system. The term w is a function of the ambient light in the water analogous to "airlight" in atmospheric propagation. The sensor noise is $n \in \mathbb{R}$.

The following assumptions are made by the author. The water medium is turbid such that visibility is on the order of a few meters. The optical imaging path relative to the object is horizontal. The object is assumed to exhibit no motion, $o_{k_1}(\mathbf{x}) = o_{k_2}(\mathbf{x}) \; \forall \; k_1$ and k_2. The optical imaging system, however, is assumed to have motion relative to the object, therefore $\tilde{\mathbf{x}}$ is kept in the imaging model.

B. Contrast Degradation

Ignoring sensor motion ($\tilde{\mathbf{x}} = \mathbf{x}$), dropping frame number k, and removing active lighting $l(\mathbf{x}) = 0 \; \forall \; \mathbf{x}$, the components that affect contrast degradation are the inside term of (1)

$$t(\mathbf{x})o(\mathbf{x}) + (1 - t(\mathbf{x}))w \quad (3)$$

The reduction of visibility underwater due to turbidity and radiant path physics are inherent optical properties (IOP) of water. Duntley [1] attributes the degradation to beam scattering (beam-c) [6] which is a summation of attenuation α_a and scattering α_s such that

$$t(\mathbf{x}) = e^{-(\alpha_a(\mathbf{x},r) + \alpha_s(\mathbf{x},r))}, \quad (4)$$

where r is the range from the optical sensor to the object.

With an active light source ($l(\mathbf{x}) = 1 \; \forall \; \mathbf{x}$), the backscatter b_b is a summation of probabilities that photons return from their incident direction when hitting water b_{bw} and particles b_{bp} [7]. These are functions of the volume scattering function $\beta(\theta)$ and half-angle θ,

$$b_b = b_{bw} + b_{bp} = 2\pi \int_{\pi/2}^{\pi} (\beta_{bw}(\theta) + \beta_{bp}(\theta)) \sin\theta d\theta. \quad (5)$$

With no ambient light and an active light source ($l(\mathbf{x}) = t(\mathbf{x}) = 1 \; \forall \; \mathbf{x}$), a similar model can be found in [8] where the observed image is a summation of direct and backscatter light $o(\mathbf{x}) + b(\mathbf{x})$.

The backscatter b_b is a function of the volume scattering functions for both water and small particles. There is also backscatter from larger particles b_{ms} which the author will call "marine snow" as is such the term used in [9]. These larger particles reflect the active light back to the sensor causing partial occlusions of the object. Similar to atmospheric snow, these occlusions are a function of many factors such as particle size, range and velocity with respect to the imaging system [9], [10]. The total backscattering component is then

$$b(\mathbf{x}) = b_b(\mathbf{x}) + b_{ms}(\mathbf{x}), \quad (6)$$

where b_b is from volumetric scattering and b_{ms} is occlusions from marine snow.

C. Optical Transfer Function

The model for the PSF in the atmosphere is discussed first so that similarities in PSFs between the two mediums (water and atmosphere) can be demonstrated. This is an important comparison because the CETM which is designed for reducing atmospheric blur is directly applied to underwater imaging with minimal modifications.

In any camera/lens system, the PSF should be included in modeling the image due to diffraction limitations. In the atmosphere, the point spread function is also (and most commonly dominated) by the random fluctuations of index of refraction along the light propagating path which is often called atmospheric turbulence. The author refers the reader to [11]–[13] for detailed discussions and models for the point spread functions related to the atmospheric turbulence. Instead of observing the PSF, it is easier to view the frequency domain representation which is the optical transfer function (OTF). Thus $h(x) = \mathcal{F}^{-1}(H(\mathbf{u}))$, where H is the OTF, $\mathbf{u}$ is the spatial frequency, and $\mathcal{F}(\cdot)$ is the inverse Fourier transform.

In summary for a horizontal imaging path and long exposure times (greater than 5ms depending on wind velocity and heat), the OTF for the atmosphere is [12], [13]

$$H_{atm}(\mathbf{u}, \lambda) = e^{-\frac{1}{2}6.88\left(\frac{\lambda f}{r_0}|\mathbf{u}|\right)^{5/3}}, \quad (7)$$

where $\mathbf{u} \in \mathbb{R}^2$ is the spatial frequency (cycles/unit distance), λ is the wavelength, f is the focal length of the imaging system, and r_0 is the atmospheric coherence diameter, or "Fried" parameter. A very small r_0 indicates severe turbulence. For a horizontal imaging path, the relationship between the Fried parameter and the atmospheric refractive index structure parameter C_n^2 is

$$C_n^2 = \frac{0.16\lambda^2}{r_0^{5/3} r} \quad (8)$$

where the range r[1] is the path from the object to the sensor. Let's reduce the parameter space in (7) using (8)

$$H_{atm}(\mathbf{u}) = e^{K_{atm}|\mathbf{u}|^{5/3} r}, \quad (9)$$

with $K_{atm} = \frac{-(1/2)6.88\lambda^{-1/3}}{0.16} C_n^2 f^{5/3}$.

In [4], a "Simple Underwater Imaging Model" (SUIM) is presented. The SUIM is an OTF representation for underwater which is a product of three OTFs; path radiance, particle

[1]Note that the range is notated with r which is common for underwater propagation models and the term r_0 is very common for denoting the Fried parameter.

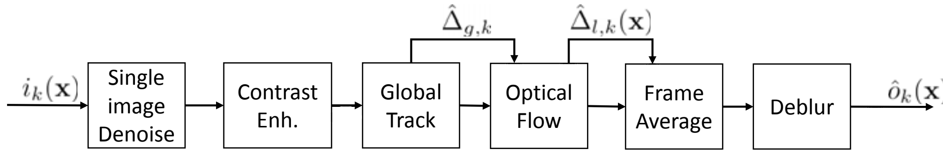

Fig. 1. Design of proposed method.

scattering, and turbulence. The complete OTF from the SUIM for horizontal path imaging is

$$H_{SUIM}(\mathbf{u}) = \left(\frac{1}{1+D}\right)\exp\left(-cr + b\frac{1-e^{-2\pi\theta_0|\mathbf{u}|}}{2\pi\theta_0|\mathbf{u}|}r\right) \times \exp\left(-S_n|\mathbf{u}|^{5/3}r\right), \quad (10)$$

where D is the path radiance, c is the beam attenuation coefficient (beam-c), b is the scattering coefficient, θ_0 is the mean scattering angle, and S_n is the Reducing the parameter space we have

$$H_{SUIM}(\mathbf{u}) = \exp\left(K_w(\mathbf{u}, r) - S_n|\mathbf{u}|^{5/3}r\right), \quad (11)$$

with the SUIM parameter $K_w(\mathbf{u}, r) = \log\left(\frac{1}{1+D}\right) - cr + b\frac{1-e^{-2\pi\theta_0|\mathbf{u}|}}{2\pi\theta_0|\mathbf{u}|}r$. The structure parameter S_n is analogous to C_n^2 in that S_n is dependent on salinity, kinetic energy, and turbulence dissipation rate of temperature [14]. Note that if $K_w(\mathbf{u}) \ll S_n = 0\ \forall\ \mathbf{u}$ the SUIM OTF approximately becomes the same form as the atmospheric OTF in (9) with dependence on $|\mathbf{u}|^{5/3}r$.

II. Proposed Method

The goal is to develop a method to enhance the incoming image stream $i_k(\mathbf{x})$ by estimating the object image $\hat{o}_k(\mathbf{x})$. In Fig. 1, the overall design of the proposed method is shown in block diagram form. This proposed method is based on the CETM method in [5]. The author refers the reader to [5] to observe the mathematical reasoning for the placement of each component of the enhancement pipeline. Since the CETM was designed for atmospheric propagation, modifications were made to accommodate underwater propagation.

A. Constrast Enhancement

In [5], a defogging method was used to enhance the contrast of the image sequence. A similar defogging method was also used by Carlevaris-Bianco et al. [15] to enhance the contrast of images underwater. In this work, the SSR-WIN system is in locations where light levels are low and lamps are used to illuminate the object of interest. This changes the contrast model where instead of

$$t(\mathbf{x})o(\mathbf{x}) + (1 - t(\mathbf{x}))w,$$

with $l(\mathbf{x}) = 0$ in (1), the backscattering is also present ($l(\mathbf{x}) > 0$)

$$t(\mathbf{x})o(\mathbf{x}) + (1 - t(\mathbf{x}))w + l(\mathbf{x})b(\mathbf{x}).$$

(a)

(b)

Fig. 2. Results of local contrast measure for images underwater. (a) Left image is contrast measure of original image, $TT(i(\mathbf{x}))$. Right image is contrast measure of enhanced image, $TT(\hat{o}(\mathbf{x}))$ (b) Left is original underwater image i. Middle is contrast enhanced image, $\hat{o}$, using the AGLG method. Right shows the pixels (red patches) in $\hat{o}$ that are above the threshold $\tau = 0.02$ where in i the threshold is below the same threshold thus indicating increased contrast for the HVS.

The author has found that instead of using a defogging method for contrast enhancement, a local contrast enhancement method proposed in [16] called Adaptive Gray-level Grouping (AGLG) was more effective in increasing the contrast automatically. The number of bins set for the AGLG enhancement filter was set to 100 for all experiments.

An objective contrast measure was applied to images for verification of effective contrast enhancements. The objective measure was proposed by Tadmor and Tolhurst [17]. The Tadmor and Tolhurst contrast measure (TT) is designed to mimic the human vision system (HVS) by measuring local contrast as illustrated in Fig. 2. In all experiments, the center masking was set to a size of 5 pixels and the surrounding mask was set to 11 pixels. With TT as the Tadmor and Tolhurst metric, the image contrast comparison for the purpose of determining contrast enhancement improvement is

$$m_{TT}(i, o) = \frac{1}{N}\sum_{\forall \mathbf{x}}\left[TT(\hat{o}(\mathbf{x})) > \tau\right] - \frac{1}{N}\sum_{\forall \mathbf{x}}\left[TT(i(\mathbf{x})) > \tau\right], \quad (12)$$

where the number of pixels in the image is N, and the contrast threshold $\tau = 0.02$ was used [18] which is a common threshold for the HVS.

B. Marine Snow Reduction

In the proposed method, the images have noise removed first with a spatial median operator of size 3×3. Then the contrast is enhanced with the AGLG filter. Next the images are aligned globally just like in [5] where the adaptive correlation filter in [19] is used to estimate Δ_g. The local motion, Δ_l, is estimated with the same optical flow method used in [5].

The difference in the proposed method compared to the method in [5] is that he frame averaging method is a temporal median filter as opposed to an average filter. The choice of a median filter (temporal domain) is chosen to not only reduce temporal noise and turbulence but also eliminate marine snow. This choice of using a median filter in the temporal domain to reduce the presence of 'snow' artifacts is also used in [10] and [9].

C. Deblur

For a preliminary investigation, the same deblurring method from [5] is used in this proposed method. The kernel for deblurring is the same form as in (9). This effectively is assuming that $K_w(\mathbf{u}) \ll S_n = 0 \ \forall \ \mathbf{u}$ which is discussed in Section I-C.

III. Results

The SSR-WIN system was deployed in the San Diego bay near the SS Curtiss in the Mole Pier Naval Base San Diego and also near Pier 160 at SSC Pacific and video sequences of pylons and anodes were recorded. Each recording was processed with the proposed method outlined in Fig. 1.

Just like the CETM method, the proposed modified CETM method receives a video sequence and generates a video sequence. But for comparisons, frames from the video sequences are presented. The before and after results of a pylon is in Fig. 3 and a comparison of the enhancement of an anode on the SS Curtiss is in Fig. 4.

Although not observable in this article, the video sequence of the anode (Fig. 4) exhibited severe marine snow with relatively large particles moving at high velocities. The frame averaging with the median operator was sufficient in reducing the occlusions b_{ms} in the images.

Although the deblurring method was designed for atmospheric blur, the enhanced frames are noticeably sharper compared to the original frames. The author does not suggest the assumption $K_w(\mathbf{u}) \ll S_n = 0 \ \forall \ \mathbf{u}$ is valid but noticeable improvements can be made when using a deblurring kernel similar to the form (9).

IV. Conclusion and Future Work

The author investigates the imaging model for underwater propagation and compares it to imaging in the atmosphere. Differences and similarities in contrast degradation are enumerated where underwater imaging additionally suffers from backscatter when active lighting is used (not including range gating systems). The PSF viewed in the frequency domain is also compared between the SUIM and the atmospheric OTF.

This work is a preliminary investigation of applying the CETM designed for atmospheric propagation to underwater imagery. Modifications were made to the CETM where the contrast enhancement method was changed from a defogging method to the AGLG method to accommodate backscattering effects caused by active lighting. Additionally, a temporal median filter was used instead of a temporal averaging filter for the frame averaging step to reduce the presence of marine snow.

A test of the method was applied to imagery obtained in San Diego bay. Results show that the modified CETM is an effective method in increasing contrast, minimizing the presence of marine snow, and sharpening the images.

In future work, the deblurring method will be modified to include the term $K_w(\mathbf{u}, r)$ from (11) to investigate an improvement in increasing sharpness for underwater imagery.

Acknowledgment

The author would like to thank the Joint Improvised Explosive Device Defeat Organization (JIEDDO) for funding this research effort.

References

[1] S. Q. Duntley, "Light in the Sea," *Journal of the Optical Society of America*, vol. 53, no. 2, p. 214, Feb. 1963.

[2] W. Wells, "Theory of small angle scattering," *Optics of the Sea*, no. I, 1973. [Online]. Available: http://www.dtic.mil/cgi-bin/GetTRDoc?AD=AD0767474#page=258

[3] J. W. McLean and K. J. Voss, "Point spread function in ocean water: comparison between theory and experiment." *Applied optics*, vol. 30, no. 15, pp. 2027–2030, 1991.

[4] W. Hou, "A simple underwater imaging model." *Optics letters*, vol. 34, no. 17, pp. 2688–2690, 2009.

[5] K. Gibson and T. Nguyen, "An analysis and method for contrast enhancement turbulence mitigation," *Image Processing, IEEE Transactions on*, vol. 23, no. 7, pp. 3179–3190, July 2014.

[6] W. Hou, *Ocean Sensing and Monitoring: Optics and Other Methods*. SPIE Press, 2013.

[7] E. Boss and W. S. Pegau, "Relationship of light scattering at an angle in the backward direction to the backscattering coefficient," *Applied Optics*, vol. 40, no. 30, pp. 5503–5507, 2001.

[8] M. Gupta, S. G. Narasimhan, and Y. Y. Schechner, "On controlling light transport in poor visibility environments," *26th IEEE Conference on Computer Vision and Pattern Recognition, CVPR*, 2008.

[9] C. a. Gamroth, "Automatic Detection and Tracking in Underwater Environments with Marine Snow," no. December, 2010.

[10] H. Hase, K. Miyake, and M. Yoneda, "Real-time snowfall noise elimination," *Proceedings 1999 International Conference on Image Processing (Cat. 99CH36348)*, vol. 2, no. M, pp. 406–409, 1999.

[11] A. N. Kolmogorov, "The local structure of turbulence in incompressible viscous fluid for very large reynolds numbers," in *Dokl. Akad. Nauk SSSR*, vol. 30, no. 4, 1941, pp. 299–303.

[12] D. L. Fried, "Statistics of a geometric representation of wavefront distortion," *JOSA*, vol. 55, no. 11, pp. 1427–1431, 1965.

[13] R. Hufnagel and N. Stanley, "Modulation transfer function associated with image transmission through turbulent media," *JOSA*, vol. 54, no. 1, pp. 52–60, 1964.

[14] W. Hou, S. Woods, E. Jarosz, W. Goode, and A. Weidemann, "Optical turbulence on underwater image degradation in natural environments," *Applied Optics*, vol. 51, no. 14, p. 2678, 2012.

[15] N. Carlevaris-Bianco, A. Mohan, and R. Eustice, "Initial results in underwater single image dehazing," *OCEANS 2010*, pp. 1–8. [Online]. Available: http://ieeexplore.ieee.org/xpl/freeabs_all.jsp?arnumber=5664428

[16] Z. Chen, B. R. Abidi, D. L. Page, and M. A. Abidi, "Gray-level grouping (glg): An automatic method for optimized image contrast enhancement-part ii: The variations," *IEEE Trans. Image Process.*, vol. 15, no. 8, pp. 2303–2314, 2006.

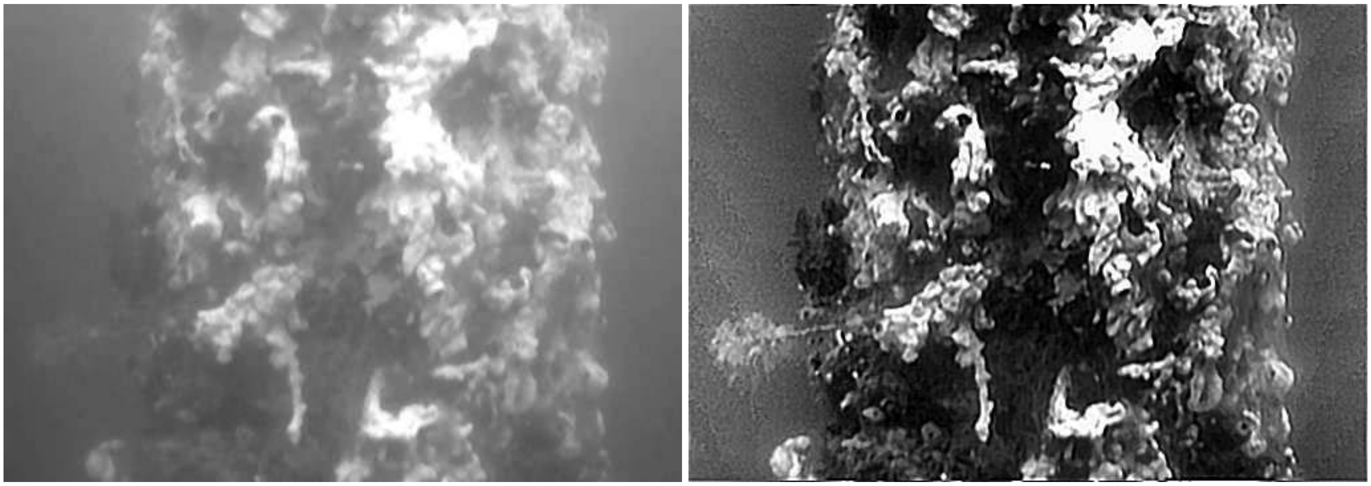

(a) (b)

Fig. 3. Results of applying the modified CETM method to a video sequence of a pylon with $r = 1m$. (a) Original frame. (b) Enhanced frame.

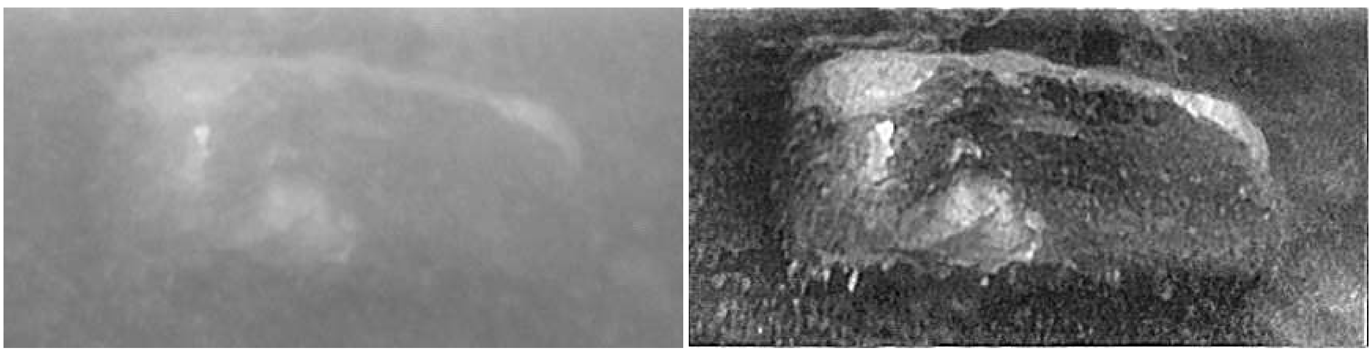

(a) (b)

Fig. 4. Results of applying the modified CETM method to a video sequence of an anode on the SS Curtiss $r = 1m$. (a) Original frame. (b) Enhanced frame.

[17] Y. Tadmor and D. Tolhurst, "Calculating the contrasts that retinal ganglion cells and lgn neurones encounter in natural scenes," *Vision research*, vol. 40, no. 22, pp. 3145–3157, 2000.

[18] W. Hou, Z. Lee, and A. D. Weidemann, "Why does the Secchi disk disappear? An imaging perspective." *Optics express*, vol. 15, no. 6, pp. 2791–2802, 2007.

[19] D. S. Bolme, J. R. Beveridge, B. A. Draper, and Y. M. Lui, "Visual object tracking using adaptive correlation filters," in *Computer Vision and Pattern Recognition, 2010 IEEE Conference on*. IEEE, 2010, pp. 2544–2550.